Valley-dependent electron retroreflection and anomalous Klein tunneling in an 8-*Pmmn* borophene-based *n-p-n* junction

Xingfei Zhou*

New Energy Technology Engineering Laboratory of Jiangsu Province, School of Science, Nanjing University of Posts and Telecommunications, Nanjing, 210023, China

(Received 26 September 2019; published 25 November 2019)

We investigate the transport properties in an 8-*Pmmn* borophene-based *n-p-n* junction. The valley-dependent electron retroreflection is generated by changing the direction of junction, which breaks up the conventional wisdom that only the electron specular reflection occurs at an interface. Furthermore, the valley-dependent anomalous Klein tunneling, i.e., the perfect transmission at a nonzero incident angle of electron regardless of the width and height of potential barrier, is found. Interestingly, this anomalous Klein tunneling depends on the direction of junction and the tilted velocity. These two findings arise from the same fact that the anisotropic band structure, induced by tilted and anisotropic velocities, leads to the release of locking relation between the transverse wave vector and velocity component along the interface. Our work gives insight into the understanding of the electron retroreflection and the Klein tunneling.

DOI: 10.1103/PhysRevB.100.195139

I. INTRODUCTION

With the successful preparation of the first two-dimensional monolayer material (graphene) [1], the other group IV two-dimensional monolayer materials, such as silicene [2], germanene [3], and stanene [4], are predicted or synthesized due to their peculiar physical and chemical properties. Furthermore, the transition metal dichalcogenides [5–9] and the group V two-dimensional monolayer materials including phosphorene [10–12], arsenene [13,14], and antimonene [14,15] have also been researched in both experiment and theory widely. Recently, the group III two-dimensional monolayer materials including borophene and aluminene are focused [16]. Particularly, the borophene with different phases are discussed widely. For example, 2-*Pmmn*, β_{12}, and χ_3 phases of borophene have been synthesized on Ag substrate under ultrahigh-vacuum conditions [17–19]. Moreover, the 8-*Pmmn* borophene has been predicted by the first-principles calculations [20]. Its effective low-energy Dirac-like Hamiltonian at the vicinity of k_D or $-k_D$ point has been proposed based on the tight-binding model [21,22], which hosts tilted and anisotropic Dirac cones. Owing to this unique band structure of 8-*Pmmn* borophene, it attracts many researchers to investigate its mechanical property [21], Weiss oscillation [23], anisotropic plasmons [24], optical property [25], RKKY exchange interaction [26], and metal-insulator transition [27]. Here we discuss the electron retroreflection and Klein tunneling in the 8-*Pmmn* borophene-based *n-p-n* junction, shown in Figs. 1(a) and 1(b).

In quantum transport progress, the phenomenon of particle reflection including retroreflection and specular reflection at an interface exists on the principle of conservation of momentum parallel to the interface universally. Generally, the type of electron reflection is the specular type in the isotropic materials due to the fact that the group velocity component parallel to the interface (u_y) is locked to the transverse wave vector k_y, shown in Fig. 1(c). In contrast, in the anisotropic materials, the anisotropic band structure releases the locking relation between u_y and k_y, which makes the electron retroreflection possible, shown in Fig. 1(d). It has been reported that the electron retroreflection can be found in Bernal-stacked and twisted graphene bilayer-based normal-superconducting junctions [28,29], respectively. However, this superconducting interface is difficult to realize in experiment. In the present paper, on account of the tilted and anisotropic Dirac cones, the 8-*Pmmn* borophene is a natural anisotropic material and the preparation of the *n-p* interface is very mature, which is suited to probe the electron retroreflection.

The Klein tunneling describes a perfect tunneling phenomenon of a relativistic electron at the normal incidence regardless of the width and height of potential barriers, which is in contrast to the conventional nonrelativistic tunneling where the transmission probability of electron exponentially decays with the increasing of the width and height of potential barriers [30,31]. Although the Klein tunneling was proposed several decades ago, the research about it almost remained stagnant until in 2006, Katsnelson designed a graphene-based *n-p-n* junction to test this unique tunneling phenomenon [32], which brought a huge wave of research in theory and experiment [33–37]. Furthermore, the anomalous Klein tunneling, i.e., the perfect tunneling with nonnormal incidence of electron, was described in a black phosphorus superlattices-based *n-p-n* junction [38], Dirac-Weyl fermion systems with tilted energy dispersion [39], and the 8-*Pmmn* borophene-based *p-n* junction [40]. Here we deepen the study of the anomalous Klein tunneling in an 8-*Pmmn*

*Corresponding author: zxf@njupt.edu.cn

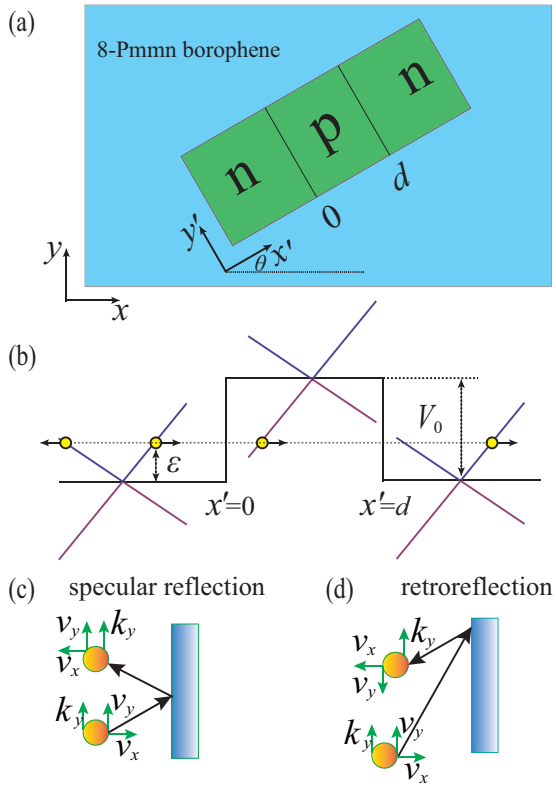

FIG. 1. (a) Top view of the proposed experimental setup for transport measurements. The blue background represents the 8-*Pmmn* borophene. The direction of *n-p-n* junction is characterized by θ. (b) The band structures in *n* and *p* regions. The incident energy of the electron is denoted by ε. The width and height of the potential barrier is d and V_0, respectively. The schematic diagrams for specular reflection and retroreflection of electron in (c) and (d), respectively.

borophene-based *n-p-n* junction and give a clear physical picture on it.

The paper is organized as follows. In Sec. II, the model and basic formalism are constructed and derived. In Sec. III, the numerical results and theoretical analysis are presented and discussed. Finally, in Sec. IV, the main results of this work are summarized.

II. MODEL AND FORMALISM

We consider the 8-*Pmmn* borophene-based *n-p-n* junction shown in Fig. 1. The Hamiltonian of the *n-p-n* junction is

$$H_\eta = \eta(\hbar v_x \sigma_x k_x + \hbar v_y \sigma_y k_y + \hbar v_t \sigma_0 k_y) + V\sigma_0. \quad (1)$$

Here the anisotropic velocities are $v_x = 0.86v_F$ and $v_y = 0.69v_F$, tilted velocity is $v_t = 0.32v_F$ with $v_F = 10^6 m/s$, $\eta = +(-)$ represents $k_D(-k_D)$ valley index [21], $\sigma_{x,y}$ and σ_0 denote the Pauli matrix and unit matrix, respectively. $V = V_0\Theta(x')\Theta(d - x')$ with the Heaviside step function Θ, the electric potential in the middle region of *n-p-n* junction, can be adjusted by gate voltage or doping. The energy dispersion is

$$E_\pm^\eta = V + \eta\hbar v_t k_y \pm \sqrt{(\hbar v_x k_x)^2 + (\hbar v_y k_y)^2}, \quad (2)$$

where $+(-)$ denotes conduction (valence) band. According to the transformation between vector components in coordinate systems $x - y$ and $x' - y'$, the relation of the wave-vector components in these two coordinate systems are

$$\begin{aligned} k_x &= k_{x'}\cos\theta - k_{y'}\sin\theta \\ k_y &= k_{x'}\sin\theta + k_{y'}\cos\theta. \end{aligned} \quad (3)$$

Then, in coordinate system $x' - y'$, the wave functions in the left, right, and middle regions are

$$\begin{aligned} \Psi_{\rm L} &= \psi_{\rm L}^i + r\psi_{\rm L}^r, \\ \Psi_{\rm M} &= a\psi_{\rm M}^i + b\psi_{\rm M}^r, \\ \Psi_{\rm R} &= t\psi_{\rm R}^t, \end{aligned} \quad (4)$$

where r is the reflection coefficient, t is the transmission coefficient, and a (b) is the incident (reflection) coefficient in the middle region. According to the Appendix, the incident, reflected, and transmitted wave functions in each region are

$$\begin{aligned} \psi_{\rm L}^{i(r)} &= \left(1, \eta\frac{\hbar v_x k_x^{i(r)} + i\hbar v_y k_y^{i(r)}}{\varepsilon - \eta\hbar v_t k_y^{i(r)}}\right)^T e^{i(k_{x'}^{i(r)}x' + k_{y'}y')}, \\ \psi_{\rm M}^{i(r)} &= \left(1, \eta\frac{\hbar v_x q_x^{i(r)} + i\hbar v_y q_y^{i(r)}}{\varepsilon - \eta\hbar v_t q_y^{i(r)} - V_0}\right)^T e^{i(q_{x'}^{i(r)}x' + k_{y'}y')}, \\ \psi_{\rm R}^{t} &= \left(1, \eta\frac{\hbar v_x k_x^{t} + i\hbar v_y k_y^{t}}{\varepsilon - \eta\hbar v_t k_y^{t}}\right)^T e^{i(k_{x'}^{t}x' + k_{y'}y')}, \end{aligned} \quad (5)$$

where T represents the transformation of matrix, ε is the incident energy of electron, the magnitudes of $k_{x'}^{i(r,t)}$ and $k_{y'}$ meet $\varepsilon = E_+^\eta$ while the magnitudes of $q_{x'}^{i(r,t)}$ and $k_{y'}$ meet $\varepsilon = E_-^\eta$, and $k_x^{i(r,t)}$, $k_y^{i(r,t)}$, $q_x^{i(r,t)}$, and $q_y^{i(r,t)}$ can be calculated by Eq. (3). Then, according to the continuity of wave function, the wave functions at the interface of the *n-p-n* junction meet

$$\Psi_{\rm L}(0) = \Psi_{\rm M}(0),\ \Psi_{\rm M}(d) = \Psi_{\rm R}(d), \quad (6)$$

and the corresponding valley-dependent transmission coefficient is written as

$$t_\eta = \frac{(A_i - A_r)(B_i - B_r)}{(A_i - B_i)(A_r - B_r)e^{iq_{x'}^i d} + (B_i - A_r)(A_i - B_r)e^{iq_{x'}^r d}}, \quad (7)$$

where

$$\begin{aligned} A_{i(r)} &= \eta\frac{\hbar v_x k_x^{i(r)} + i\hbar v_y k_y^{i(r)}}{\varepsilon - \eta\hbar v_t k_y^{i(r)}}, \\ B_{i(r)} &= \eta\frac{\hbar v_x q_x^{i(r)} + i\hbar v_y q_y^{i(r)}}{\varepsilon - \eta\hbar v_t q_y^{i(r)} - V_0}. \end{aligned} \quad (8)$$

According to the conservation of probability current in the Appendix, the valley-dependent transmission probability across the *n-p-n* junction is written as $T_\eta = t^* t$.

III. RESULTS AND DISCUSSION

A. Valley-dependent electron retroreflection

In a coordinate $x' - y'$ system, the velocity of an electron is defined as $u = \frac{1}{\hbar}\nabla_k E$. So the valley-dependent velocity

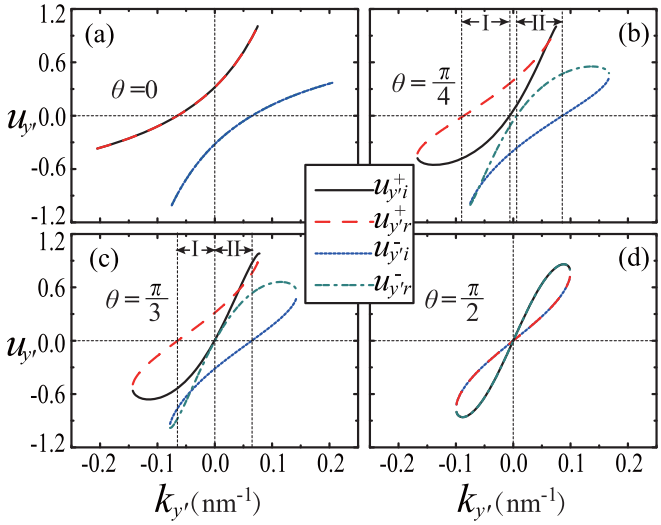

FIG. 2. (a)–(d) Transverse wave vector $k_{y'}$-dependent transverse velocity $u_{y'}$ with the incident energy of electron $\varepsilon = 0.05$ eV. Here $u^{+}_{y'i(r)}$ denotes the transverse velocity of incident (reflected) electron from $\mathbf{k}_D$ valley while $u^{-}_{y'i(r)}$ denotes the transverse velocity of incident (reflected) electron from $-\mathbf{k}_D$ valley. The unit for all transverse velocities is v_F.

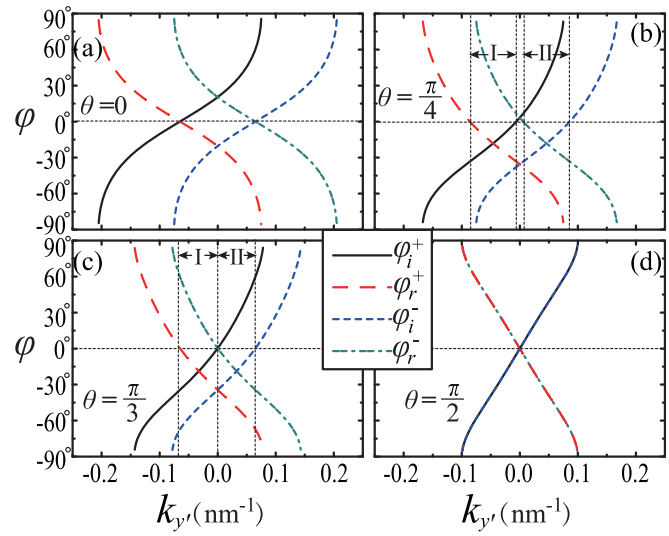

FIG. 3. (a)–(d) Transverse wave vector $k_{y'}$-dependent incident (reflected) angle of incident (reflected) electron with $\varepsilon = 0.05$ eV. Here $\varphi^{+}_{i(r)}$ denotes the incident (reflected) angle of electron from $\mathbf{k}_D$ valley while $\varphi^{-}_{i(r)}$ denotes the incident (reflected) angle of electron from $-\mathbf{k}_D$ valley.

components are calculated as

$$u^{\eta}_{x'} = \frac{\partial E^{\eta}_{+}}{\hbar \partial k_{x'}} = \eta v_t \sin\theta + \frac{v_x^2 k_x \cos\theta + v_y^2 k_y \sin\theta}{\sqrt{k_x^2 v_x^2 + k_y^2 v_y^2}},$$
$$u^{\eta}_{y'} = \frac{\partial E^{\eta}_{+}}{\hbar \partial k_{y'}} = \eta v_t \cos\theta + \frac{-v_x^2 k_x \sin\theta + v_y^2 k_y \cos\theta}{\sqrt{k_x^2 v_x^2 + k_y^2 v_y^2}}. \quad (9)$$

Then the valley-dependent incident (reflected) angle of electron is

$$\varphi^{\eta}_{i(r)} = \arctan \frac{u^{\eta}_{y'i(r)}}{u^{\eta}_{x'i(r)}}. \quad (10)$$

Given the transverse wave vector $k_{y'}$ and the incident energy ε, we can obtain the longitudinal wave vector $k_{x'i}$ ($k_{x'r}$) of incident (reflected) electron from Eqs. (2) and (3). Then the valley-dependent transverse velocity $u^{\eta}_{y'i}$ ($u^{\eta}_{y'r}$) of incident (reflected) electron can be calculated by Eqs. (9), which is shown in Fig. 2 with $\theta = 0, \pi/4, \pi/3$, and $\pi/2$. According to the schematic diagrams for specular reflection and retroreflection of electron in Figs. 1(c) and 1(d), the same (opposite) directions of transverse velocities of incident and reflected electrons is corresponding to the specular reflection (retroreflection). Due to the same sign of $u^{\eta}_{y'i}$ and $u^{\eta}_{y'r}$ in Figs. 2(a) and 2(d), the electron retroreflection is absent in $\theta = 0$ and $\pi/2$. However, in Figs. 2(b) and 2(c), retroreflection of electron from k_D ($-k_D$) valley is generated in the I (II) region. For the consideration of experiment, we give the transverse wave vector $k_{y'}$-dependent incident (reflected) angle of incident (reflected) electron, shown in Fig. 3. Because of the opposite sign of φ^{η}_{i} and φ^{η}_{r} in Figs. 3(a) and 3(d), only electron specular reflection happens. Obviously, the retroreflection of electron from k_D ($-k_D$) valley is generated in I (II) region in Figs. 3(b) and 3(c). This valley-dependent electron retroreflection phenomenon comes from the release of locking relation between the transverse wave vector $k_{y'}$ and the velocity component along the interface $u^{\eta}_{y'}$, shown in Eq. (9).

B. Valley-dependent anomalous Klein tunneling

In the coordinate $x' - y'$ system, we rewrite the Hamiltonian [Eq. (1)]

$$H_\eta = \eta(\hbar S_x k_{x'} + \hbar S_y k_{y'}) + V\sigma_0, \quad (11)$$

where S_x and S_y are defined in Eq. (A2). The velocity operator along the x' direction is $\hat{u}_{x'} = \frac{1}{i\hbar}[x', H_\eta] = \eta S_x$. Its time evolution is given by the Heisenberg equation of motion:

$$\dot{\hat{u}}_{x'} = \frac{1}{i\hbar}[\hat{u}_{x'}, H_\eta] = 2v_x v_y \sigma_z k_{y'}. \quad (12)$$

Obviously, the velocity along x' is conserved when $k_{y'} = 0$, which means the appearance of perfect transmission ($T_\eta = 1$ for $k_{y'} = 0$) regardless of the width and height of potential barrier. We calculate the $k_{y'}$-dependent transmitted probability in different parameters, shown in Fig. 4, to verify our analysis. From the discussion above, we can give a conclusion that the conservation of $u_{x'}$ in the case of $k_{y'} = 0$ ensures the Klein tunneling of electron.

The general transmitted probability in the n-p-n junction is solved through Eq. (7). When $\theta = 0$, the valley-dependent transmitted probability is simplified as

$$T_\eta = \frac{1}{\cos^2 q_x d + \chi^2 \sin^2 q_x d}, \quad (13)$$

where $\chi = \frac{\chi_L^2 + \chi_M^2}{2\chi_L\chi_M} \sec\alpha \sec\beta - \tan\alpha \tan\beta$ with $\chi_L = \eta\Theta(\varepsilon - \eta\hbar v_t k_y)$, $\chi_M = \eta\Theta(\varepsilon - \eta\hbar v_t k_y - V_0)$, $\alpha = \arctan(v_y k_y / v_x k_x)$, and $\beta = \arctan(v_y k_y / v_x q_x)$. Here k_x is the longitudinal wave vector in two n regions, and q_x is the longitudinal wave vector in the p region. In the graphene-based n-p-n junction, the

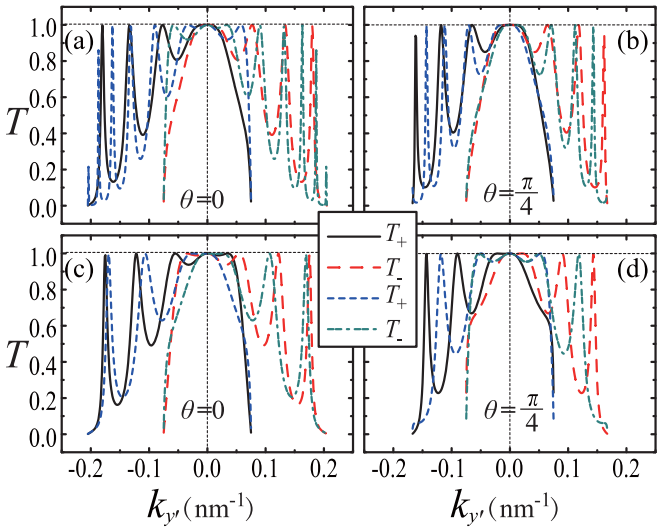

FIG. 4. (a)–(d) Transverse wave vector $k_{y'}$-dependent transmission probability with $\varepsilon = 0.05$ eV. The black and red lines (blue and green lines) are plotted with the parameters $V_0 = 0.3\,(0.2)$ eV and $d = 100$ nm in (a) and (b). The black and red lines (blue and green lines) are plotted with the parameters $V_0 = 0.3$ eV and $d = 90\,(80)$ nm in (c) and (d). Here $T_{+(-)}$ represents the transmission probability of electron from $\mathbf{k}_D$ ($-\mathbf{k}_D$) valley.

Klein tunneling only occurs in the case of normal incidence of electron due to the fact that the incident angle of electron is α and is equal to zero when $k_y = 0$. However, in our model, the azimuthal angle of wave vector is not equal to the one of velocity. From Eq. (10), we obtain the incident angle of electron in the case of $\theta = 0$

$$\varphi_i^{\eta} = \arctan \frac{\eta v_t + v_y \sin\alpha}{v_x \cos\alpha}. \tag{14}$$

It is easy to find that the Klein tunneling occurs at the incident angle $\varphi_i^{\eta} = \eta v_t / v_x \approx \eta 20.4^{\circ}$, which is shown in Fig. 5(a).

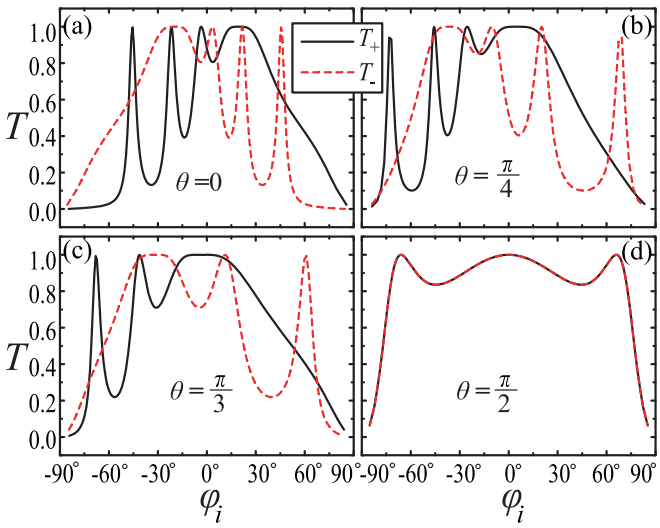

FIG. 5. (a)–(d) Transmission probability versus the incident angle of electron with the parameters $V_0 = 0.3$ eV and $d = 100$ nm. Here $T_{+(-)}$ represents the transmission probability of the electron from the $\mathbf{k}_D$ ($-\mathbf{k}_D$) valley.

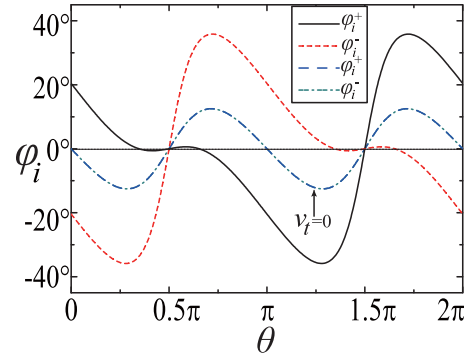

FIG. 6. Valley-dependent incident angle of electron φ_i^{η} of Klein tunneling versus the direction of junction θ with $k_{y'} = 0\varepsilon = 0.05$ eV, $d = 100$ nm, and $V_0 = 0.3$ eV. Here the blue and green lines are plotted in the assumption of $v_t = 0$.

Compared with the case of the graphene-based *n-p-n* junction, there are two differences: One is the nonzero incident angle-induced Klein tunneling; the other is the valley-dependent Klein tunneling. These two peculiar properties arise from the tilted energy dispersion. From Eq. (14), it is easy to see that the phenomenon of Klein tunneling in our model is the same as the one in the graphene system when the tilted term $v_t = 0$.

In the case of $\theta = \frac{\pi}{4}$, when $k_{y'} = 0$, the incident angle of electron from k_D ($-k_D$) valley $\varphi_{y'i}^{+(-)} \approx 3.26^{\circ}$ (-35.54°) by calculating Eq. (10). Similarly, $\varphi_{y'i}^{+(-)} \approx 0.28^{\circ}(-34.46^{\circ})$ in the case of $\theta = \frac{\pi}{3}$. At these incident angles, the phenomenon of Klein tunneling happens, which arises from the anisotropic band structure and is consistent with that in Figs. 5(b) and 5(c). In the case of $\theta = \frac{\pi}{2}$, the incident angle-dependent transmitted probability is plotted in Fig. 5(d). We can find that the incident angle of Klein tunneling is zero, which is the same as the one in the graphene-based *n-p-n* junction. When $k_{y'} = 0$, $u_{y'}^{\eta} = 0$ from Eq. (9) obviously, which leads to the appearance of Klein tunneling at zero incident angle. Besides these special angles, in Fig. 5, there are other angles for $T^{\eta} = 1$, which is the phenomenon of resonant tunneling of electron. These resonant angles are sensitive to the incident energy ε, the width and height of potential barrier, and the direction of junction.

For the sake of discussion, we define an asymmetric parameter $\gamma = \frac{v_x}{v_y}$. If the tilted velocity $v_t = 0$ and $\gamma = 1$, then the Klein tunneling in our model is the same as the one in the graphene system obviously. If tilted velocity is not equal to zero, then the nonzero incident angle-dependent Klein tunneling appears regardless of the value of γ, which can be seen from Eq. (14) easily. If the tilted velocity $v_t = 0$ but $\gamma \neq 1$, then the nonzero incident angle-dependent Klein tunneling also appears, shown in Fig. 6. However, the range of nonzero incident angle of Klein tunneling is narrower than the one in the case of $v_t \neq 0$. From the energy dispersion in Eq. (2) and the discussion above, the tilted velocity or the asymmetric parameter ($\gamma \neq 1$) can make the band structure anisotropic, which is key to realize the nonzero incident angle-dependent Klein tunneling.

Through the calculations and analysis above, the Klein tunneling can occur at the different valley-dependent incident angles in different directions of junction (different θ) due to the anisotropic band structure inducing the release of the locking relation between $u_{y'}$ and $k_{y'}$. This phenomenon is named as valley-dependent anomalous Klein tunneling, which provides a new perspective for understanding Klein tunneling.

IV. CONCLUSIONS

In conclusion, we investigate the valley-dependent electron retroreflection and anomalous Klein tunneling in an 8-*Pmmn* borophene-based *n*-*p*-*n* junction. In the low energy Hamiltonian, the tilted velocity and the asymmetric parameters make the band structure anisotropic, which leads to the release of locking relation between the transverse wave vector and velocity component along the interface and then makes the valley-dependent electron retroreflection and anomalous Klein tunneling realizable. The electron retroreflection can only be generated by changing the direction of junction while the anomalous Klein tunneling directly appears without the change of the direction of junction due to the tilted velocity. Interestingly, the nonzero incident angle of anomalous Klein tunneling can be adjusted by changing the direction of junction. The phenomena in the present paper are general and applicable to any anisotropic Dirac fermion systems and give a new perspective for understanding the electron reflection and the Klein tunneling.

ACKNOWLEDGMENTS

This work was supported by the National Natural Science Foundation of China (Grants No. 11747019, No. 11804167, No. 11804291, and No. 61874057), the Natural Science Foundation of Jiangsu Province (Grants No. BK20180890 and No. BK20180739), the Universities Natural Science Research Project of Jiangsu Province (Grant No. 17KJB140031), the Innovation Research Project of Jiangsu Province (Grant No. CZ0070619002), and NJUPT-SF (Grant No. NY218128).

APPENDIX: THE PROCESS FOR DERIVING THE WAVE FUNCTION AND PROBABILITY CURRENT

1. Calculation of wave function

In the coordinate $x'-y'$ system, the Hamiltonian of an 8-*Pmmn* borophene is rewritten as

$$H_\eta = \eta(\hbar S_x k_{x'} + \hbar S_y k_{y'}) + V\sigma_0, \tag{A1}$$

where

$$\begin{aligned} S_x &= v_x\sigma_x\cos\theta + v_y\sigma_y\sin\theta + v_t\sigma_0\sin\theta, \\ S_y &= -v_x\sigma_x\sin\theta + v_y\sigma_y\cos\theta + v_t\sigma_0\cos\theta. \end{aligned} \tag{A2}$$

In the coordinate representation, $k_{x'} \to -i\frac{\partial}{\partial x'}$ and $k_{y'} \to -i\frac{\partial}{\partial y'}$, then the Schrödinger equation is $H_\eta\psi = \varepsilon\psi$. Inserting a trial wave function $\psi = (1, m)^T e^{i(k_{x'}x' + k_{y'}y')}$ into the Schrödinger equation, we obtain the trial wave function

$$\psi = \begin{pmatrix} 1 \\ \eta\frac{\hbar v_x k_x + i\hbar v_y k_y}{\varepsilon - \eta\hbar v_t k_y - V} \end{pmatrix} e^{i(k_{x'}x' + k_{y'}y')}. \tag{A3}$$

2. Derivation of probability current

The time-dependent Schrödinger equation and its conjugate equation are written as

$$i\hbar\frac{\partial\psi}{\partial t} = -i\eta\hbar\left(S_x\frac{\partial}{\partial x'} + S_y\frac{\partial}{\partial y'}\right)\psi, \tag{A4}$$

$$-i\hbar\frac{\partial\psi^\dagger}{\partial t} = i\eta\hbar\left(S_x\frac{\partial}{\partial x'} + S_y\frac{\partial}{\partial y'}\right)\psi^\dagger. \tag{A5}$$

Through $\psi^\dagger\times$Eq. (A4)-$\psi\times$Eq. (A5) and the probability density $\rho = \psi^\dagger\psi$, we obtain the equation of the conservation of probability current

$$\frac{\partial\rho}{\partial t} + \nabla\cdot\mathbf{J} = 0, \tag{A6}$$

where $\mathbf{J} = \eta(\psi^\dagger S_x\psi, \psi^\dagger S_y\psi)$ is the probability current. In our paper, the probability current is conserved in the x' direction, then the incident probability current $J_{x'i} = \eta\psi_i^\dagger S_x\psi_i$ and the transmitted probability current $J_{x't} = \eta t^* t\psi_t^\dagger S_x\psi_t$, so the transmitted probability is $T = \frac{J_{x't}}{J_{x'i}} = t^* t$ due to $\psi_t = \psi_i$ in our model.

[1] K. S. Novoselov, A. K. Geim, S. V. Morozov, D. Jiang, M. I. Katsnelson, I. V. Grigorieva, S. V. Dubonos, and A. A. Firsov, Nature (London) **438**, 197 (2005).
[2] C.-C. Liu, H. Jiang, and Y. Yao, Phys. Rev. B **84**, 195430 (2011).
[3] M. E. Dávila, L. Xian, S. Cahangirov, A. Rubio, and G. Le Lay, New J. Phys. **16**, 095002 (2014).
[4] F. Zhu, W. Chen, Y. Xu, C. Gao, D. Guan, C. Liu, D. Qian, S.-C. Zhang, and J. Jia, Nat. Mater. **14**, 1020 (2015).
[5] Q. H. Wang, K. Kalantar-Zadeh, A. Kis, J. N. Coleman, and M. S. Strano, Nat. Nanotechnol. **7**, 699 (2012).
[6] A. Scholz, T. Stauber, and J. Schliemann, Phys. Rev. B **88**, 035135 (2013).
[7] X. Xu, W. Yao, D. Xiao, and T. F. Heinz, Nat. Phys. **10**, 343 (2014).
[8] Y. Li, A. Chernikov, X. Zhang, A. Rigosi, H. M. Hill, A. M. van der Zande, D. A. Chenet, E.-M. Shih, J. Hone, and T. F. Heinz, Phys. Rev. B **90**, 205422 (2014).
[9] S. Manzeli, D. Ovchinnikov, D. Pasquier, O. V. Yazyev, and A. Kis, Nat. Rev. Mater. **2**, 17033 (2017).
[10] L. Li, Y. Yu, G. Jun Ye, Q. Ge, X. Ou, H. Wu, D. Feng, X. Hui Chen, and Y. Zhang, Nat. Nanotechnol. **9**, 372 (2014).
[11] H. Liu, A. T. Neal, Z. Zhu, Z. Luo, X. Xu, D. Tomanek, and P. D. Ye, ACS Nano **8**, 4033 (2014).
[12] A. Carvalho, M. Wang, X. Zhu, A. S. Rodin, H. Su, and A. H. Castro Neto, Nat. Rev. Mater. **1**, 16061 (2016).
[13] C. Kamal and M. Ezawa, Phys. Rev. B **91**, 085423 (2015).
[14] Z. Zhang, Z. Yan, Y. Li, Z. Chen, and H. Zeng, Angew. Chem. Int. Ed. **54**, 3112 (2015).

[15] J. Ji, X. Song, J. Liu, Z. Yan, C. Huo, S. Zhang, M. Su, L. Liao, W. Wang, Z. Ni, Y. Hao, and H. Zeng, Nat. Commun. **7**, 13352 (2016).
[16] C. Kamal, A. Chakrabarti, and M. Ezawa, New J. Phys. **17**, 083014 (2015).
[17] A. J. Mannix, X. F. Zhou, B. Kiraly, J. D. Wood, D. Alducin, B. D. Myers, X. Liu, B. L. Fisher, U. Santiago, J. R. Guest, M. J. Yacaman, A. Ponce, A. R. Oganov, M. C. Hersam, and N. P. Guisinger, Science **350**, 1513 (2015).
[18] B. Feng, J. Zhang, Q. Zhong, W. Li, S. Li, H. Li, P. Cheng, S. Meng, L. Chen, and K. Wu, Nat. Chem. **8**, 563 (2016).
[19] W. Li, L. Kong, C. Chen, J. Gou, S. Sheng, W. Zhang, H. Li, L. Chen, P. Cheng, and K. Wu, Sci. Bull. **63**, 282 (2018).
[20] A. Lopez-Bezanilla and P. B. Littlewood, Phys. Rev. B **93**, 241405(R) (2016).
[21] A. D. Zabolotskiy and Y. E. Lozovik, Phys. Rev. B **94**, 165403 (2016).
[22] M. Nakhaee, S. A. Ketabi, and F. M. Peeters, Phys. Rev. B **97**, 125424 (2018).
[23] S. K. Firoz Islam and A. M. Jayannavar, Phys. Rev. B **96**, 235405 (2017).
[24] K. Sadhukhan and A. Agarwal, Phys. Rev. B **96**, 035410 (2017).
[25] S. Verma, A. Mawrie, and T. K. Ghosh, Phys. Rev. B **96**, 155418 (2017).
[26] G. C. Paul, S. K. Firoz Islam, and A. Saha, Phys. Rev. B **99**, 155418 (2019).
[27] A. E. Champo and G. G. Naumis, Phys. Rev. B **99**, 035415 (2019).
[28] Y. S. Ang, Z. Ma, and C. Zhang, Sci. Rep. **2**, 1013 (2012).
[29] Y. Xu and G. Jin, Solid State Commun. **247**, 72 (2016).
[30] O. Klein, Z. Phys. **53**, 157 (1929).
[31] A. Calogeracos and N. Dombey, Contemp. Phys. **40**, 313 (1999).
[32] M. I. Katsnelson, K. S. Novoselov, and A. K. Geim, Nat. Phys. **2**, 620 (2006).
[33] M. A. Zeb, K. Sabeeh, and M. Tahir, Phys. Rev. B **78**, 165420 (2008).
[34] A. Rozhkov, G. Giavaras, Y. P. Bliokh, V. Freilikher, and F. Nori, Phys. Rep. **503**, 77 (2011).
[35] H. Oh, S. Coh, Y.-W. Son, and M. L. Cohen, Phys. Rev. Lett. **117**, 016804 (2016).
[36] N. Stander, B. Huard, and D. Goldhaber-Gordon, Phys. Rev. Lett. **102**, 026807 (2009).
[37] P. E. Allain and J. N. Fuchs, Eur. Phys. J. B **83**, 301 (2011).
[38] Z. Li, T. Cao, M. Wu, and S. G. Louie, Nano Lett. **17**, 2280 (2017).
[39] V. H. Nguyen and J.-C. Charlier, Phys. Rev. B **97**, 235113 (2018).
[40] S.-H. Zhang and W. Yang, Phys. Rev. B **97**, 235440 (2018).